Chemical Science

EDGE ARTICLE

View Article Online
View Journal | View Issue

Cite this: *Chem. Sci.*, 2015, **6**, 3900

Multiscale electrochemistry of hydrogels embedding conductive nanotubes†

Jean-Marc Noël,‡[a] Léopold Mottet,‡[b] Nicolas Bremond,[b] Philippe Poulin,[c] Catherine Combellas,[a] Jérôme Bibette[b] and Frédéric Kanoufi*[a]

Received 12th February 2015
Accepted 2nd April 2015

DOI: 10.1039/c5sc00549c

www.rsc.org/chemicalscience

The local functionalities of biocompatible objects can be characterized under conditions similar to the operating ones, using scanning electrochemical microscopy (SECM). In the case of alginate beads entrapping carbon nanotubes (CNTs), SECM allows evidencing of the local conductivity, organization, and communication between the CNTs. It shows that the CNT network is active enough to allow long range charge evacuation, enabling the use of alginate/CNT beads as soft 3D electrodes. Direct connection or local interrogation by a microelectrode allows visualization of their communication as a network and eventually the study of them individually at the nanoscale.

Introduction

Hydrogels are soft materials mainly composed of water embedded in a polymeric matrix. Their wide range of applications, from the food industry and drug delivery[1] to tissue engineering,[2] and their rich physicochemical features make them appealing from both fundamental and applied viewpoints. Most hydrogels are biocompatible by nature and are thus well suited for biotechnology uses. As for other polymer based materials, mixing two kinds of macromolecule charges offers extra properties to the final composite such as stretchability[3] or electrical conductivity.[4]

In a different way, conductive hybrid hydrogels can be obtained by dispersing mineral charges, such as carbon nanotubes.[5] Moreover, incorporating conductive particles opens the way to advanced conducting materials for energy storage,[6,7] biosensors[8] or synthetic tissues.[9] In the design of such smart functional materials, it is then important to assess the availability of their functionalities, particularly *in situ* while they are operated. Owing to the various shapes, softness and composition (>90% of water) of hydrogels, SEM or AFM are much less well adapted for imaging their structure without physical disturbance than Scanning Electrochemical Microscopy, SECM, since for SEM, water has to be removed, whilst for AFM, there is contact between the tip and the surface. Conversely, SECM is an *in situ* local (electro) chemical probe technique that is well adapted to smart soft object imaging. SECM successfully allows the characterization of soft spherical objects, such as polymeric microbeads[10] or vesicles.[11–13] Regarding permeable materials, SECM is able (i) to reveal ion transport through a nanoporous membrane,[14] with capability for preferential transport path imaging,[15] or (ii) to quantify local conductive sites at an interface.[16,17] Local electrochemical probe microscopy techniques, such as SECM or scanning electrochemical cell microscopy (SECCM), are ideal to characterize *in situ* the conductive properties of materials such as CNT based materials going from single CNTs[17,18] to CNT networks.[19–21] Only a few approaches have been reported to study the electrochemical activity of CNTs, or other graphene-like materials, mixed with polymers,[22,23] even though CNTs offer promising strategies for the development of novel methodologies for the formulation of energy storage materials.

Herein, we have focused on auto-organized spherical soft objects engineered from carbon nanotubes (CNTs) and an alginate biopolymer, owing to a millifluidic dropping method. We have quantified and imaged *in situ* the active sites of such as-formed functional permeable objects using SECM. The ultramicroelectrode (UME) tip of the SECM will be especially used to (i) probe the actuable hydrogel beads under the operation conditions, (ii) quantify the increase in conductivity upon CNT incorporation, (iii) characterize the organization of the conductive network, and (iv) show how it can be used to directly address or connect the conductive network.

[a]*Sorbonne Paris Cité, Paris Diderot University, Interfaces, Traitements, Organisation et Dynamique des Systèmes (ITODYS), CNRS-UMR 7086, 15 rue J. A. de Baif, 75013 Paris, France. E-mail: frederic.kanoufi@univ-paris-diderot.fr; Fax: +33 157277263; Tel: +33 157277217*

[b]*Laboratoire Colloïdes et Matériaux Divisés, Institute of Chemistry, Biology and Innovation (CBI) – ESPCI ParisTech/CNRS-UMR8231/PSL* Research University, 10 rue Vauquelin 75231, Paris Cedex, France*

[c]*Centre de Recherche Paul Pascal – CNRS, University of Bordeaux, 115 Avenue Schweitzer, 33600 Pessac, France*

† Electronic supplementary information (ESI) available: Alginate/carbon nanotube bead fabrication and optical image, SECM approach curves in benzonitrile, 2D conductivity images, SECM of the tip penetrating inside the bead and Digisim® simulation of cyclic voltammograms obtained at an UME inside a 1% CNT bead. See DOI: 10.1039/c5sc00549c

‡ The first two authors contributed equally to this work.

Results and discussion

SECM approach toward a conductive permeable hydrogel

As described in the ESI (Fig. S1†), multi-walled carbon nanotubes are sonicated with sodium dodecylsulfate then mixed with alginate. This solution is dropped into a calcium bath to create alginate/CNT beads. Such 3 mm diameter alginate beads, modified with different percentages of CNTs (0 to 1 wt%), were characterized using SECM in the feedback mode in a solution containing a redox mediator, namely ferrocene methanol (FcMeOH) (Fig. 1A). In this mode, an UME tip oxidizes the redox mediator while it is approaching the alginate bead. Far from the object, it produces a steady-state current (i_{inf}) that is limited by redox mediator diffusion. In the vicinity of the object and if the latter has conductive properties, the redox mediator is regenerated to its pristine state, yielding a feedback current at the UME tip. The evolution of the normalized tip current, $I = i/i_{inf}$, with the tip-object separation distance, d (also in a normalized form $L = d/a$ with a as the UME tip radius), gives the so-called approach curve. As alginate beads are biocompatible and mostly used in aqueous media, the analysis of their conductive properties is performed in water. Indeed, SECM approach curves for the beads were obtained in a KCl medium containing FcMeOH as the redox mediator.

The approach curve recorded for an alginate bead free of CNTs (Fig. 1B, thick light green curve, O) is different from the one corresponding to classical insulating behavior.[15] This difference is attributed to the partition of FcMeOH between the aqueous phase and the hydrogel, and its transport in both phases. Indeed, an approach curve recorded for a hydrogel bead from a water-immiscible solvent (benzonitrile, BZN), with a hydrophobic redox mediator (decamethylferrocene, DcFc, Fig. S2†), presents insulating behavior (negative feedback), which means that the redox mediator does not permeate the alginate bead and no charge transfer occurs at the alginate/BZN interface. Thus, as proposed in earlier work,[24–28] the partition process can be quantitatively described through finite element methods modeling (Comsol) of the approach curve. In the absence of CNTs, the experimental curve fits well to a theoretical insulating porous behavior (Fig. 1B, black line).

When CNTs are added inside the hydrogel beads (from 0.13 to 1 wt%), the approach curves show higher feedback currents than in the former insulating case, as the redox mediator is regenerated at the alginate/CNT bead surface (Fig. 1B). A feedback current is detected at the tip for a CNT concentration as low as 0.13 wt%, and this feedback increases with the CNT concentration.

A quantitative estimate of the feedback and therefore of the apparent interfacial charge transfer for each bead composition is provided by modelling the data for the permeation of the redox species in the alginate bead phase and the interfacial electron transfer process (regeneration of FcMeOH) at the water/bead interface. The permeation takes into account the higher reservoir of the redox mediator provided by the bead. The apparent interfacial ET reasonably averages the contribution from regeneration within the volume of the bead. As a first approach, we believe that this model is sufficient. Indeed, owing to the size of the UME (25 μm diameter) and the diffusion coefficient of the redox mediator within the hydrogel, which is about 3 times lower than in aqueous media, the redox mediator will be regenerated from within 10 μm deep inside the hydrogel and could be considered as a weak contribution to the homogeneous phase. This simple theoretical framework yields a reasonable fit of the experimental approach curves, as shown in Fig. 1B. It is noteworthy that some deviation between the experimental and the fitted approach curve can be observed, in Fig. 1B, for the bead containing 0.3% CNTs. This could suggest that the regeneration of the redox mediator outside the area of the UME is limited. This imbalance could be created in the case of inhomogeneous repartition or accessibility of the CNTs at the surface (as attested later by the SECM image provided in Fig. 2A) or inside the bead. This could be paralleled to systems for which the probed conductor is not much larger than the tip.[29] However, this interpretation is at this point speculative and probably true only for a low percentage of CNTs since at 1% CNTs the accessibility of the CNTs is homogeneous (as also confirmed by the SECM image discussed later, Fig. 2B).

Even if a more refined model considering homogeneous charge transfer within the bead phase and requiring at least 2 other adjustable parameters would be more complete, the fit provided by the simplest model is reasonable, as was also suggested in other related systems combining layers of polymers embedding CNTs. Moreover, in the literature, the irreversible charge transfer model appeared to be a well adapted approach to study nanoparticles or carbon nanotubes trapped at various interfaces.[19,30–35] More notably, the apparent charge transfer rate constant determined from the approach curve fitting increases linearly with the percentage of CNTs trapped inside the hydrogel. Moreover, the increase of FcMeOH concentration does not increase the charge transfer rate (not shown). These observations on the charge transfer process at the bead surface upon CNT incorporation suggest that conductive sites, likely CNTs arranged in a nanoelectrode network, are now exposed and available at the bead surface to the solution phase. As the bead is not connected to any electrical source, the observation of a

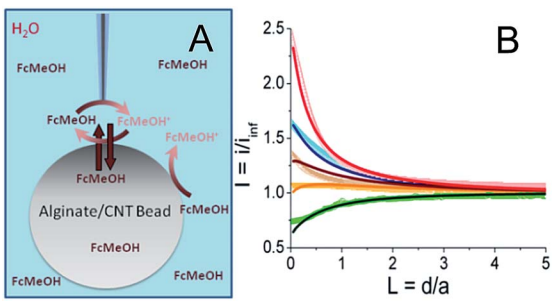

Fig. 1 (A) Principle of the SECM approach curves for a 2 mm diameter alginate/CNT bead in a 0.1 M KCl + 1 mM $CaCl_2$ aqueous solution containing 1 mM FcMeOH. (B) Approach curves recorded with a 12.5 μm Pt UME tip toward alginate beads containing CNTs: 0 (O), 0.13 (O), 0.3 (□), 0.55 (□), and 1 (□) wt%. Lines are the simulated curves for irreversible electron transfer kinetics. k_{el} = 0, 1.82, 3.65, 6.08 and 12.2 $\times 10^{-3}$ cm^{-1} for, respectively, 0, 0.13, 0.3, 0.55 and 1 wt%, using $D = 7.8 \times 10^{-6}$ cm s^{-1} for the diffusion coefficient of FcMeOH in water.

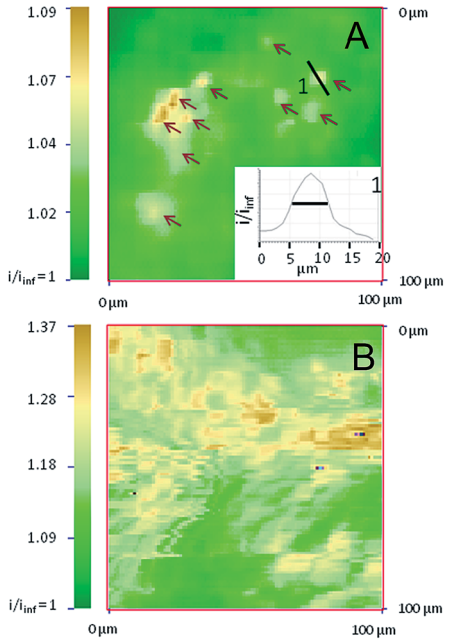

Fig. 2 SECM images of alginate/CNT beads containing (A) 0.3 and (B) 1 wt% CNTs recorded in a 0.1 M KCl + 1 mM $CaCl_2$ aqueous solution containing 1 mM FcMeOH. Using a 400–500 nm radius Pt nanotip at a 10 µm s^{-1} velocity. The nanotip was kept less than 1 µm from the surface. The current scale was normalized using the steady state current recorded in the bulk solution. In (A), the arrows point to the 10 most conductive spots and the inset shows the current profile along the black line of one spot.

steady-state charge transfer at the bead surface also indicates that upon redox mediator regeneration (reduction of $FcMeOH^+$ by the CNTs), charges (electrons and ions) are readily propagated within the bead to be evacuated toward the solution or deeper into the bead (by the oxidation of FcMeOH, see Fig. 1A) at distances larger than the UME tip size.

2D SECM conductivity images

SECM also allows imaging of the distribution of the reactive sites responsible for the surface conductivity of the outer membrane of the alginate/CNT beads. Using the same 12.5 µm radius UME tip, an image from the apex of a bead containing 0.55 wt% CNTs (Fig. S3A†), recorded in a FcMeOH aqueous medium, presents a homogeneous conductivity (in line with the reproducibility of the approach curves performed at different locations). With a nanoelectrode (nanotip, 400–500 nm radius),[36,37] a higher resolution is expected for the electrochemical image of the bead. Few individual small conductive spots with 5–10 µm FWHM diameter (~6 µm, in inset) are revealed for beads containing 0.3 wt% of CNTs, as shown in Fig. 2A, whereas the density of these active regions significantly increases when the CNT wt% entrapped inside the gel increases to 0.55 (Fig. S3B†) and 1 wt% (Fig. 2B).

At low concentrations of CNTs, the SECM images show that only a few agglomerates are exposed directly to the external solution and work as a network of individual microelectrodes. Assuming each spot acts as an individual microelectrode, their size can be estimated from the maximum feedback they sustain (measured from Fig. 2A),[38] and can be compared to the theoretical values obtained from finite element methods modeling (Comsol). Typically, the ten intense spots resolved in Fig. 2A with i/i_{inf} values in the 1.03–1.09 range (see arrows) correspond to feedback responses of individual microelectrodes separated by 1 µm from a 1 µm diameter nanotip with an apparent diameter in the 1–1.5 µm range. This is in reasonable agreement with Fig. 2A since, due to convolution with the tip size, the SECM image of these individual microelectrodes would ideally be of 2–3 µm diameter active spots.

It is noteworthy that the density of these active sites (40–50 μm^2 over a 10^4 μm^2 image) is within the 0.3% density of the CNTs incorporated in the bead. The spacing between each of these active spots is higher than the nanotip dimension used for their imaging in Fig. 2A. This strongly suggests that if these spots are detected electrochemically with both 1 and 12.5 µm radius tips, they are connected to each other for charge evacuation.

The contrast and density of the apparent active sites revealed in the SECM images also reflect the overlapping of the diffusion layers generated by the network of microelectrodes formed by the CNT assemblies. It allows imaging of the individual location of the spots and also their range of cross-talk. For a low concentration of CNTs, overlapping of the diffusion layers of the microelectrode network is evidenced and limited to the upper part of Fig. 2A. The increase of the CNT concentration results in an apparent increase of the number of conductive spots and significant overlapping of the diffusion cross-talk, as shown in Fig. S3B† and 2B for 0.55 and 1 wt% CNT beads respectively. The feedback ($1.09 < i/i_{inf} < 1.37$) recorded over the whole imaged surface is significant and compares to the maximum expected current for a positive feedback for tip-to-bead separation distance $d = 1$ or 0.5 µm ($i/i_{inf} = 1.25$ or 1.57, respectively). The full regeneration of the redox mediator at the bead is then detected by the SECM nanotip over regions expanding over several tens of μm^2, showing the large interpenetration of the active spots' fields of action. This then suggests that the bead with 1 wt% CNTs is comparable to an array of nanoelectrodes, which behave as a "macroelectrode", owing to the overlapping of the individual diffusion layers.[31,39] These features, which are shown in Fig. 2B, could then reveal the topography of the macroelectrode and therefore the topography of the bead surface, where the regions of higher current are overhanging by as much as 1 µm in the lower current regions. The differences between Fig. 2A and B further suggest that the CNT assembly is homogeneously distributed at high CNT concentrations and more segregated at lower concentrations. Finally, both SECM images and approach curves show that the CNTs entrapped in an alginate bead behave as macro- or micro-electrode arrays. Definitely, such an observation requires that charge evacuation occurs efficiently within the bead, certainly through a percolated CNT network entrapped within the hydrogel. If micro- or nano-electrochemical probes allow evidencing and imaging of the structure of the CNT percolation in the hydrogel beads, the macroscopic range of the charge transfer (or percolation) within the bead can be explored by direct electrical connection of the bead.

Connection to a conductive network

Penetrating the UME tip inside the bead allows inspection of the extent of the conductive network within the alginate bead. The approach curve from the solution to the bead interior is depicted in Fig. S4† where the solution/bead interface is indicated as a red vertical line; the deeper the penetration into the bead, the higher the feedback current. At ~50 μm penetration inside the bead, the tip current increases by several orders of magnitude (from 2 nA in the solution to several μA), suggesting that the UME tip has electrically connected the CNT percolated network. It is then no longer possible to interrogate the microenvironment of the tip, only the entire range of the percolated network functioning as a macroelectrode.

One benefit of using a UME for this connection is the large increase of current from the transition between microelectrode and macroelectrode behaviour. Another is the ability to reversibly connect the percolated network without too much physical perturbation of the object (Experimental details in ESI†).

It is interesting to note here that no significant increase in the current was detected during the connection to 0.13, 0.3 and 0.5 wt% CNT beads, traducing the efficient percolation detected between 0.5 and 1 wt%.

The principle behind the connection between the UME tip and the CNT network in a 1 wt% CNT bead is illustrated in Fig. 3A together with the resulting cyclic voltammogram (CV) of the FcMeOH oxidation (Fig. 3B). It would be interesting to compare the charge transfer capacities of the beads obtained using the probe approach curves, Fig. 1, at different concentrations of CNTs with CVs recorded at different CNT content; unfortunately it was not possible to properly connect the conducting network with the UME for a concentration below 1%, probably because of the limited accessibility of the CNT network at a low percentage of CNTs and a higher resistance of the bead. This particularly highlights the unique potentiality of SECM to address the electrochemical activity of such soft objects with low conductivity.

The CV of a bead containing 1 wt% CNT (Fig. 3B) shows the classical response expected for a macroelectrode, except that the peak to peak separation potential, $\Delta E_p = 536$ mV at $v = 100$ mV s^{-1}, is much higher than the theoretical value obtained at a classical metallic electrode for a diffusion process ($\Delta E_p = 60$ mV). This behavior illustrates a large charge transfer resistance probably due to a limited accessibility of the deeper regions of the CNT network. However, this experiment clearly shows the possibility to connect the CNT network trapped inside the hydrogel. The peak current (I_p) also varies linearly with $v^{1/2}$ (inset in Fig. 3B). Even if the electrochemical response shows considerable ohmic contribution, the $I_p - v^{1/2}$ response may suggest a diffusion-controlled limitation. From this experiment and using a FcMeOH diffusion coefficient in alginate of $D_{FcMeOH/Alg} = 2.9 \times 10^{-6}$ cm^2 s^{-1}, both the equivalent resistance and surface area of the connected 1 wt% CNT network can be estimated from simulation of the CVs (see ESI†). The UME–bead electrical contact is equivalent to a 3.3 mm^2 electrode of 80 kΩ resistance. This means that by coming into contact with the bead, the active area of the UME tip used as a connector is multiplied by 6.7×10^3. Such a significant increase shows a volumetric percolation of the CNT network through the bead. Of course, since the cyclic voltammetry was conducted in an aqueous medium and due to the high permeability of the bead, the CV may result from the response of a volume fraction of the bead.

A further picture of the electrochemical characteristics for the alginate/CNT bead was obtained by separating the outer surface and the bulk bead contributions. For this purpose, a bead was equilibrated in a hydroquinone (HQ) solution and then immersed into a BZN electrolyte containing DcFc as a redox mediator (Fig. 3C). The CV obtained by the same electrical connection to an UME tip (Fig. 3D) shows two reversible waves corresponding to the response of both the redox mediator (DcFc in the BZN phase) and HQ (inside the hydrogel). This clearly shows that it is possible to connect the outer surface of the bead with its interior (the electrode was inserted <100 μm inside the bead), showing a long distance percolation range of the CNT network. A more quantitative estimate of the equivalent electroactive surface area is obtained for the outer surface (from the DcFc CV) and the volumetric network (from the HQ CV) of the bead from the respective peak current analysis. This ensures that 0.3 mm^2 of the external surface of the bead is active (using $D_{DcFc/BZN} = 4.6 \times 10^{-6}$ cm^2 s^{-1} for DcFc diffusion in BZN), which corresponds to 1% of the surface of the bead. Due to the large overlapping of the active nanodomains formed by the CNT network evidenced by SECM, this value suggests that the electrical connection is effective for electrochemical measurements over the 1% area in the vicinity of the electrical connection. Typically, the UME tip addresses here an electrically connected region equivalent to a 0.3 mm radius disk electrode. Conversely, the part of the CNT network connected within the interior of the bead has an active area of 0.8 mm^2 (considering $D_{HQ/Alg} =$

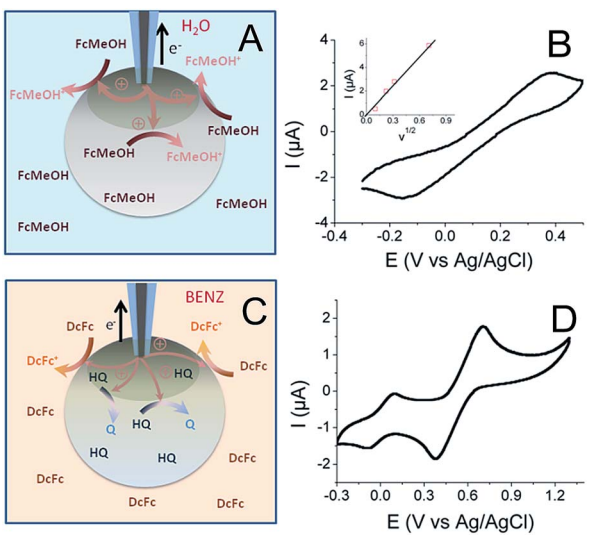

Fig. 3 (A and C) Principle of the direct connection of an alginate bead with a 12.5 μm radius UME tip. (B and D) Cyclic voltammograms recorded at a scan rate of $v = 100$ mV s^{-1} for a 3 mm diameter alginate bead containing 1 wt% CNTs: (B) in a 0.1 M KCl + 1 mM FcMeOH aqueous solution (inset: peak current, I_p, as a function of $v^{1/2}$); (D) equilibrated with an aqueous solution of 1 mM hydroquinone (HQ) and immersed into a 1 mM DcFc + 0.1 M NBu_4BF_4 BZN solution.

$D_{FcMeOH/Alg} = 2.9 \times 10^{-6}$ cm^2 s^{-1}). The electrically connected alginate/CNT bead then behaves as a macroscopic porous electrode. From the area connected at the outer surface, it is anticipated that the electrical connection inside the bead expands only over a hemisphere of similar radius (0.3 mm). Such a percolated porous electrode then behaves as a 0.3 mm hemisphere electrode, leading to a 2-fold increase of the inside electroactive area, in reasonable agreement with the 2.6-fold increase observed.

Conclusions

These preliminary investigations show the ability of SECM to characterize the availability of physical or chemical functionalities of smart, soft, biocompatible objects, under conditions similar to their operating ones, without physical perturbation, which is very important for maintaining the structure of the composite. Thus, approach curves obtained with an UME tip at the surface of a hydrogel bead entrapping CNTs allow easy characterization of their local conductivity. High resolution SECM imaging clearly evidences the local availability, organization, and communication of the functional objects entrapped within the composite (here CNT modified hydrogel beads). At low content, the CNTs assemble in individual segregated bundles of approx. 5 μm in diameter. The bead is then not conductive enough to be addressed electrochemically by cyclic voltammetry, which highlights the unique proficiency of SECM for the electrochemical characterization of such poorly conductive soft objects. At higher concentrations, the CNT distribution is more homogeneous and the bead is a dense overlapping network of nanoelectrodes, which behaves as a rough macroelectrode. In all cases, the CNT network is active enough to allow long range charge evacuation, enabling the use of alginate/CNT beads as soft 3D electrodes. This is confirmed from the direct connection of the CNT network to the UME tip. It is then possible to address, with a 12.5 μm radius UME inserted inside the bead, the whole electrical volume or surface in a liquid/liquid environment within a range of 300 μm from the tip–bead contact. The use of this 3D biocompatible hydrogel can be extended to the trapping and further electrochemical addressing of many other kinds of objects, such as nanoparticles, electroactive molecules or biological entities. The direct connection or local interrogation by microelectrodes allows visualization of their communication as a network and eventually the study of them individually at the nanoscale. The potentiality of such hydrogels in a liquid/liquid environment was also demonstrated, which is appealing in the development of soft materials for energy storage/release.

Acknowledgements

This work was supported by Université Paris-Diderot, ESPCI and CNRS.

Notes and references

1 T. R. Hoare and D. S. Kohane, *Polymer*, 2008, **49**, 1993.
2 K. Y. Lee and D. J. Mooney, *Chem. Rev.*, 2001, **101**, 1869.
3 J.-Y. Sun, X. Zhao, W. R. K. Illeperuma, O. Chaudhuri, K. H. Oh, D. J. Mooney and Z. Suo, *Nature*, 2012, **489**, 133.
4 A. Guiseppi-Elie, *Biomaterials*, 2010, **31**, 2701.
5 Z. Yang, Z. Cao, H. Sun and Y. Li, *Adv. Mater.*, 2008, **20**, 2201.
6 H. Wu, G. Yu, L. Pan, N. Liu, M. T. McDowell, Z. Bao and Y. Cui, *Nat. Commun.*, 2013, **4**, 1943.
7 B. Liu, P. Soares, C. Checkles, Y. Zhao and G. Yu, *Nano Lett.*, 2013, **13**, 3414.
8 D. Zhai, B. Liu, Y. Shi, L. Pan, Y. Wang, W. Li, R. Zhang and G. Yu, *ACS Nano*, 2013, **7**, 3540.
9 R. A. MacDonald, C. M. Voge, M. Kariolis and J. P. Stegemann, *Acta Biomater.*, 2008, **4**, 1583.
10 C. N. Kirchner, M. Träuble and G. Wittstock, *Anal. Chem.*, 2010, **82**, 2626.
11 W. Zhan and A. J. Bard, *Anal. Chem.*, 2006, **78**, 726.
12 D. Correia-Ledo, A. A. Arnold and J. Mauzeroll, *J. Am. Chem. Soc.*, 2010, **132**, 15120.
13 R. Tomasi, J.-M. Noël, A. Zenati, S. Ristori, F. Rossi, V. Cabuil, F. Kanoufi and A. Abou-Hassan, *Chem. Sci.*, 2014, **5**, 1854.
14 M. Shen, R. Ishimatsu, J. Kim and S. Amemiya, *J. Am. Chem. Soc.*, 2012, **134**, 9856.
15 *Scanning Electrochemical Microscopy*, ed. A. J. Bard and M. V. Mirkin, Taylor & Francis, New York, 2012.
16 J. Azevedo, C. Bourdillon, V. Derycke, S. Campidelli, C. Lefrou and R. Cornut, *Anal. Chem.*, 2013, **85**, 1812.
17 J. Kim, H. Xiong, M. Hofmann, J. Kong and S. Amemiya, *Anal. Chem.*, 2010, **82**, 1605.
18 A. G. Güell, K. E. Meadows, P. V. Dudin, N. Ebejer, J. V. Macpherson and P. R. Unwin, *Nano Lett.*, 2014, **14**, 220.
19 N. R. Wilson, M. Guille, I. Dumitrescu, V. R. Fernandez, N. C. Rudd, C. G. Williams, P. R. Unwin and J. V. Macpherson, *Anal. Chem.*, 2006, **78**, 7006.
20 T. S. Miller, N. Ebejer, A. G. Güell, J. V. Macpherson and P. R. Unwin, *Chem. Commun.*, 2012, **48**, 7435.
21 A. G. Güell, N. Ebejer, M. E. Snowden, K. McKelvey, J. V. Macpherson and P. R. Unwin, *Proc. Natl. Acad. Sci. U. S. A.*, 2012, **109**, 11487.
22 V. A. Pedrosa, T. Gnanaprakasa, S. Balasubramanian, E. V. Olsenc, V. A. Davis and A. L. Simonian, *Electrochem. Commun.*, 2009, **11**, 1401.
23 M. E. Snowden, M. A. Edwards, N. C. Rudd, J. V. Macpherson and P. R. Unwin, *Phys. Chem. Chem. Phys.*, 2013, **15**, 5030.
24 A. L. Barker and P. R. Unwin, *J. Phys. Chem.*, 2001, **105**, 12019.
25 P. Bertoncello, I. Ciani, D. Marenduzzo and P. R. Unwin, *J. Phys. Chem. C*, 2007, **111**, 294.
26 C. Cannes, F. Kanoufi and A. J. Bard, *Langmuir*, 2002, **18**, 8134.
27 J. Guo and S. Amemiya, *Anal. Chem.*, 2005, **77**, 2147.
28 J. Kim, A. Izadyar, N. Nioradze and S. Amemiya, *J. Am. Chem. Soc.*, 2013, **135**, 2321.
29 A. I. Oleinick, D. Battistel, S. Daniele, I. Svir and C. Amatore, *Anal. Chem.*, 2011, **83**, 4887.
30 J. Zhang, R. M. Lahtinen, K. Kontturi, P. R. Unwin and D. J. Schiffrin, *Chem. Commun.*, 2001, 1818.

31 B. M. Quinn, I. Prieto, S. K. Haram and A. J. Bard, *J. Phys. Chem. B*, 2001, **105**, 7474.
32 P. Liljeroth, D. Vanmaekelbergh, V. Ruiz, H. Jiang, E. Kauppinen and B. M. Quinn, *J. Am. Chem. Soc.*, 2004, **126**, 7126.
33 P. G. Nicholson, V. Ruiz, J. V. Macpherson and P. R. Unwin, *Phys. Chem. Chem. Phys.*, 2006, **8**, 5096.
34 F. Li, I. Ciani, P. Bertoncello, P. R. Unwin, J. Zhao, C. R. Bradbury and D. J. Fermin, *J. Phys. Chem. C*, 2008, **112**, 9686.
35 J.-M. Noël, D. Zigah, J. Simonet and P. Hapiot, *Langmuir*, 2010, **26**, 7638.
36 B. Ballesteros Katemann and W. Schuhmann, *Electroanalysis*, 2002, **14**, 22.
37 J. Velmurugan, P. Sun and M. V. Mirkin, *J. Phys. Chem. C*, 2009, **113**, 459.
38 C. Amatore, J.-M. Savéant and D. Tessier, *J. Electroanal. Chem. Interfacial Electrochem.*, 1983, **147**, 39.
39 N. Godino, X. Borrisé, F. X. Muñoz, F. J. del Campo and R. G. Compton, *J. Phys. Chem. C*, 2009, **113**, 11119.